Struct Multidisc Optim (2008) 36:43–58
DOI 10.1007/s00158-007-0169-4

RESEARCH PAPER

Topology optimization of shell structures using adaptive inner-front (AIF) level set method

Kang-Soo Park · Sung-Kie Youn

Received: 15 November 2006 / Revised: 17 April 2007 / Accepted: 18 July 2007 / Published online: 15 December 2007

Abstract A new topology optimization using adaptive inner-front level set method is presented. In the conventional level set-based topology optimization, the optimum topology strongly depends on the initial level set due to the incapability of inner-front creation during the optimization process. In the present work, in this regard, an algorithm for inner-front creation is proposed in which the sizes, the positions, and the number of new inner-fronts during the optimization process can be globally and consistently identified. In the algorithm, the criterion of inner-front creation for compliance minimization problems of linear elastic structures is chosen as the strain energy density along with volumetric constraint. To facilitate the inner-front creation process, the inner-front creation map is constructed and used to define new level set function. In the implementation of inner-front creation algorithm, to suppress the numerical oscillation of solutions due to the sharp edges in the level set function, domain regularization is carried out by solving the edge smoothing partial differential equation (smoothing PDE). To update the level set function during the optimization process, the least-squares finite element method (LSFEM) is adopted. Through the LSFEM, a symmetric positive definite system matrix is constructed, and non-diffused and non-oscillatory solution for the hyperbolic PDE such as level set equation can be obtained. As applications, three-dimensional topology optimization of shell structures is treated. From the numerical examples, it is shown that the present method brings in much needed flexibility in topologies during the level set-based topology optimization process.

Keywords Topology optimization · Level set method · Inner-front creation · LSFEM

K. S. Park · S. K. Youn (✉)
Department of Mechanical Engineering, Korea Advanced Institute of Science and Technology, 373–1, Guseong-dong, Yuseong-gu, Daejeon, 305–701, South Korea
e-mail: skyoun@kaist.ac.kr

K. S. Park
e-mail: pgsoo@kaist.ac.kr

1 Introduction

Since the pioneering work of Bendsøe and Kikuchi (1988), topology optimization method has attracted a great deal of attention of researchers and engineers and has been applied to various engineering design problems in the fields of structural optimization. Notwithstanding its rapid progress, however, the topology optimization method has left certain rooms for further improvement. In general, the obstacles encountered in applying topology optimization include the formation of checker-board patterns and the occurrence of intermediate densities (Harber et al. 1996; Youn and Park 1997; Bendsøe and Sigmund 2003).

As a new attempt to overcome the shortcomings, the level set-based topology optimization has been proposed by Sethian and Wiegmann (2000). In the level set-based topology optimization method, the moving front which corresponds to the material boundary is given as the design variable. As the material boundary evolves, it can be freely merged and/or

splitted. The evolution of material boundary is governed by the level set equation employing the shape velocity, which is computed from the design sensitivity analysis (DSA). Unlike the conventional topology optimization method, since the optimum shape is represented by the material boundary, both intermediate densities and checker-board patterns can be avoided. Based on the basic notion of the level set-based topology optimization, several application examples have been presented. Some of the examples include structural optimization problems considering linear elasticity (Wang et al. 2003), nonlinear elasticity (Allaire et al. 2004; Kwak and Cho 2005), eigenfrequency (Allaire et al. 2004), compliant mechanism (Allaire et al. 2004), multi-materials and multi-constraints (Wang and Wang 2004), and heat conduction (Ha and Cho 2005).

In the conventional level set-based topology optimization, new inner-fronts cannot be created in the material domain during the optimization process. Since some of inner-fronts are merely merged, an initial level set distribution usually includes a large number of inner-fronts, and the optimum topology of the conventional level set-based topology optimization is significantly affected by the initial distribution of inner-fronts (Allaire et al. 2004). To overcome the shortcomings, attempts to create inner-fronts during the optimization process by incorporating the topological derivative (Sokołowski and Żochowski 1999; Novotny et al. 2003) with the level set-based topology optimization have been presented. In the works, the topological derivative that relates changes in the objective function to the introduction of infinitesimally small inner-fronts is used as a criterion for inner-front creation. In the practical implementations, by removing nodes (or elements) (Céa et al. 2000), inserting soft materials (Mei and Wang 2004; Burger et al. 2004), perforating level set function (Allaire et al. 2005), or adding forcing term (Amstutz and Andra 2006) at the local regions where the topological derivative attains its extreme value, topological changes can be carried out during the optimization process.

In the present work, a new inner-front creation algorithm is proposed in which the sizes, the positions, and the number of new inner-fronts during the optimization process are adaptively and consistently identified by considering both the value of a given criterion for inner-front creation and the occupied volume of material domain. Especially, as a generalized energy density, the value of strain energy density of linear elastic structure is employed as a criterion for inner-front creation. In addition, to smooth out the sharp edges due to the abrupt changes of level set function values during the inner-front creation, an edge smoothing based on the technique of smoothing partial differential equation (smoothing PDE; Aubert and Kornprobst 2001) is carried out. As the applications of adaptive inner-front level set method, topology optimization of shell structures is dealt with. In engineering fields and industrial areas, due to the handling limitation and manufacturing cost, the total weight of structures should be kept low. However, there exist the trade-offs between stiffness and weight. In this context of lightweight design, in the present work, applying the compliance minimization problem subjected to volume constraint to the shell structures, such as the cantilever beam, curved shell structure, and steel deck, which are common applications in the field of aerospace engineering, the promising flexibility, and potential of the present method are demonstrated.

In Section 2, the level set method is briefly reviewed. In Section 3, the inner-front creation algorithm, optimization formulation, and shape design sensitivity analysis are presented. In Section 4, numerical examples of the level set-based topology optimization using adaptive inner-front creation map are presented. The emphasis is on the construction and implementation of the inner-front creation algorithm to identify the suitable sizes, positions, and number of inner-fronts in the material domain.

2 Level set method

In this section, the level set method is briefly outlined. The basic concept, mathematical model, and numerical implementation can be found in Osher and Sethian (1998), Sethian (1999), Osher and Fedkiw (2003), and references there in.

2.1 Basic concept and mathematical model

Basic idea of the level set method is to describe a curve or a surface in an implicit form as the zero level set or iso-level of a higher dimensional function. Thus, the boundary that will be denoted Γ is represented by a set of all points $\mathbf{x}$, which correspond to the zero value of level set function ϕ, as follows:

$$\Gamma = \{\mathbf{x} | \phi(\mathbf{x}, t) = 0, \quad \mathbf{x} \in \Omega\}, \tag{1}$$

where Ω denotes the analysis domain.

To describe the governing equation of the evolution of level set function, material derivative is taken on Γ. That is,

$$\begin{aligned}\frac{D\phi}{Dt} &= \frac{\partial\phi}{\partial t} + \frac{\partial \mathbf{x}}{\partial t}\cdot\nabla\phi,\\ &= \frac{\partial\phi}{\partial t} + \mathbf{V}\cdot\nabla\phi,\\ &= 0,\end{aligned} \tag{2}$$

where $\dfrac{D(\bullet)}{Dt}$ is the material derivative, t the time variable, and $\mathbf{V} \equiv \dfrac{\partial \mathbf{x}}{\partial t} = \left[V_x, V_y, V_z\right]$ the local velocity.

Using the relationship between the normal vector and level set function $\mathbf{n} = -\dfrac{\nabla\phi}{|\nabla\phi|}$, (2) can be represented as follows:

$$\frac{\partial\phi}{\partial t} - V_n\,|\nabla\phi| = 0, \tag{3a}$$

with initial condition:

$$\phi(\mathbf{x}, t = t_0) = \phi_0(\mathbf{x}), \tag{3b}$$

where $\mathbf{V}_n \equiv \mathbf{V}\cdot\mathbf{n}$ is the speed in the normal direction of boundary, and t_0 the initial time.

Equation (3a) is called the level set equation, which is a kind of Hamilton–Jacobi equation.

As shown in (2), the level set equation is derived from in the rectangular Cartesian coordinates. However, to describe the evolution of level set function in the curved domains, the level set equation should be reformulated in curvilinear coordinates $\xi^j (= [\xi, \eta, \zeta])$ in which velocity vectors follow the coordinate directions. As an illustrative example, a schematic diagram of boundary representation by the level set function in curvilinear coordinates is shown in Fig. 1. The closed curve (dashed line) in Fig. 1 represents the zero level set in curvilinear coordinates.

To convert the level set equation from Cartesian coordinates to curvilinear coordinates, the set of transformation rules adopted by Lee and Soni (1997), Takahira et al. (2004), and Yue et al. (2005) is applied. Based on the transformation rules, the level set equation in curvilinear coordinates can be obtained as follows:

$$\frac{\partial\phi}{\partial t} + \frac{1}{J}\frac{\partial}{\partial\xi^j}\left(\frac{J}{\sqrt{g_{jj}}}\phi V^j\right) = 0 \quad j = 1, \cdots, 3, \tag{4}$$

where $J = \det[J]$ is the Jacobian, $[J]$ the Jacobian matrix, $\sqrt{g_{jj}} = \sqrt{\mathbf{g}_j\cdot\mathbf{g}_j}$ the magnitude of covariant basis vector g_j in the curvilinear coordinates, and V^j the velocity component in the ξ^j-coordinate direction.

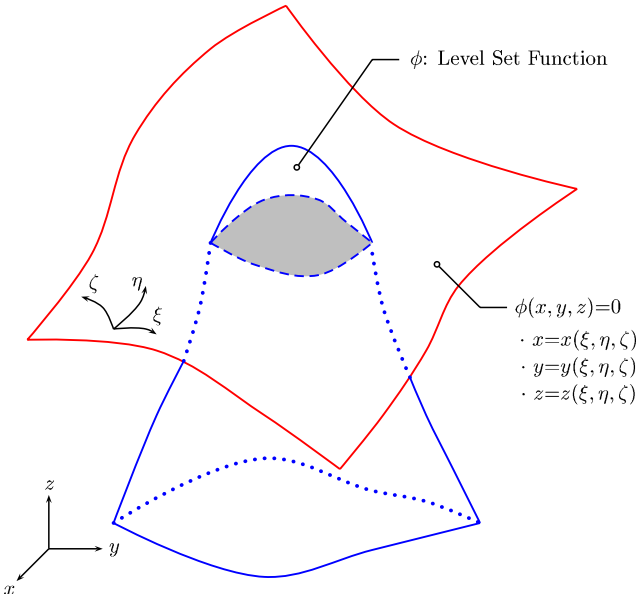

Fig. 1 Boundary representation by level set function in curvilinear coordinates

2.2 Domain representation and regularization

At an arbitrary time of level set evolution, the material and void domains can be separated by the sign of level set function values. Namely,

$$\begin{aligned}&\phi(\mathbf{x}, t) > 0 \quad \text{for } \mathbf{x} \in \Omega_{\text{MAT}},\\ &\phi(\mathbf{x}, t) = 0 \quad \text{for } \mathbf{x} \in \Gamma_{\text{MAT}},\\ &\phi(\mathbf{x}, t) < 0 \quad \text{for } \mathbf{x} \in \Omega_{\text{VOID}},\end{aligned} \tag{5}$$

where Ω_{MAT} is the material domain, Γ_{MAT} the material boundary, $\Omega_{\text{VOID}} = \Omega_{\text{DES}}\backslash\overline{\Omega_{\text{MAT}}}$ the void domain, Ω_{DES} the design domain, and $\overline{\Omega_{\text{MAT}}}$ the closure of material domain.

To serve the mathematical convenience of manipulating the material and void domains, the following Heaviside step function is used:

$$H(\varsigma) \equiv \begin{cases} 0 & \text{if } \varsigma < 0,\\ 1 & \text{if } \varsigma \geq 0.\end{cases} \tag{6}$$

The derivative of the Heaviside step function is also defined as the following Dirac delta function:

$$\delta(\varsigma) \equiv \frac{dH(\varsigma)}{d\varsigma}. \tag{7}$$

By introducing the Heaviside step and Dirac delta functions, the domain and boundary integrals of a function $F(\boldsymbol{x})$ can be expressed as follows:

$$\text{Domain integral} \quad \int_\Omega F(\boldsymbol{x})H(\phi)d\Omega, \tag{8a}$$

Boundary integral $\int_\Gamma F(\boldsymbol{x})d\Gamma = \int_\Omega F(\boldsymbol{x})\delta(\phi)\,|\nabla\phi|\,d\Omega.$ (8b)

For the numerical implementation, the Heaviside step and Dirac delta functions are regularized and replaced by the smooth and continuous functions, $H_\alpha(\varsigma)$ and $\delta_\alpha(\varsigma)$, respectively. In the present work, the following regularized Heaviside step and Dirac delta functions with regularization parameter α are employed:

$$H_\alpha(\varsigma) = \begin{cases} \Delta_S & \text{if } \varsigma < -\alpha, \\ -\dfrac{\varsigma^3}{4\alpha^3} + \dfrac{3\varsigma}{4\alpha} + \dfrac{1}{2} & \text{if } |\varsigma| \le \alpha, \\ 1 & \text{if } \varsigma > \alpha, \end{cases} \tag{9a}$$

and

$$\delta_\alpha(\varsigma) = \begin{cases} \Delta_S & \text{if } |\varsigma| > \alpha, \\ -\dfrac{3}{4\alpha}\left(\dfrac{\varsigma^2}{\alpha^2} - 1\right) & \text{if } |\varsigma| \le \alpha, \end{cases} \tag{9b}$$

where Δ_S is the small constant being used to avoid the zero stiffness (say 0.001).

Figure 2 shows the regularized step and delta functions for a certain regularization parameter α. In the computation, $\alpha = 0.5$ is used.

2.3 Computation for level set evolution

As presented in the early works of level set method, the finite difference-based techniques, such as Upwind, essentially non-oscillatory (ENO), weighted ENO, and Godunov's schemes, have been widely employed to update the level set function. The theory and application of the conventional updating schemes can be found in Sethian (1999) and Osher and Fedkiw (2003). Although the conventional updating schemes are easily applicable to regular domains and boundary conditions, they still possess certain computational difficulties when geometry and/or boundary conditions become more complicated.

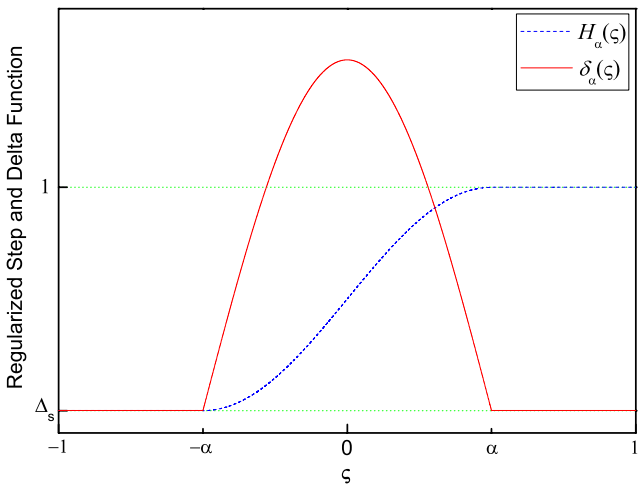

Fig. 2 Regularized Heaviside step and Dirac delta function

In the present work, the LSFEM is adopted to compute the evolution of level set function. The least-squares finite element formulation can give a symmetric positive definite system matrix for the non-self adjoint first order hyperbolic problems such as the level set equation. Thus, the conventional solution method based on the finite elements can be easily employed without any special treatment. In addition, numerical stability of LSFEM for the first order hyperbolic problem is a well-established fact. The basic theory, formulation, and application of LSFEM can be found in Jiang (1998) and references there in.

To proceed the least-squares finite element formulation of level set equation in curvilinear coordinates, the following equation is considered in a component form of (4):

$$\frac{\partial\phi}{\partial t} + \frac{1}{J}\frac{\partial}{\partial\xi}\left(\frac{J}{\sqrt{g_{11}}}V^1\phi\right) + \frac{1}{J}\frac{\partial}{\partial\eta}\left(\frac{J}{\sqrt{g_{22}}}V^2\phi\right) + \frac{1}{J}\frac{\partial}{\partial\zeta}\left(\frac{J}{\sqrt{g_{33}}}V^3\phi\right) = 0. \tag{10}$$

A least-squares formulation of (10) can be obtained as the following procedure:

For a given time step $\Delta t = t^{k+1} - t^k$, (10) is discretized with the backward difference scheme in time as follows:

$$\phi^{k+1} - \phi^k + \frac{\Delta t}{J}\left[\frac{\partial}{\partial\xi}\left(\frac{J}{\sqrt{g_{11}}}V^{1k}\phi^{k+1}\right) + \frac{\partial}{\partial\eta}\left(\frac{J}{\sqrt{g_{22}}}V^{2k}\phi^{k+1}\right) + \frac{\partial}{\partial\zeta}\left(\frac{J}{\sqrt{g_{33}}}V^{3k}\phi^{k+1}\right)\right] = 0, \tag{11}$$

where k denotes the k-th time step.

Equation (11) can be represented as the following matrix form:

$$\mathbf{A}^{k+1}\phi^{k+1} = \mathbf{r}^{k+1}, \tag{12}$$

where

$$\mathbf{A}^{k+1} = \left[1 + \frac{\Delta t}{J}\left(\frac{JV^{1k}}{\sqrt{g_{11}}}\frac{\partial}{\partial\xi} + \frac{JV^{2k}}{\sqrt{g_{22}}}\frac{\partial}{\partial\eta} + \frac{JV^{3k}}{\sqrt{g_{33}}}\frac{\partial}{\partial\zeta}\right)\right],$$

$$\phi^{k+1} = \left[\phi^{k+1}\right],$$

$$\mathbf{r}^{k+1} = \left[\phi^k\right].$$

Applying the least-squares formulation with the test function $\varphi \in \mathbf{H}^1(\Omega)$, the energy bilinear and load linear forms to solve (12) are constructed as follows:

$$\mathbf{B}(\phi, \varphi) = \mathbf{R}(\varphi) \quad \text{for all } \varphi \in \mathbf{H}^1(\Omega), \tag{13}$$

where

$$\mathbf{B}(\phi, \varphi) \equiv \left(\mathbf{A}^{k+1}\phi^{k+1}, \mathbf{A}^{k+1}\varphi\right),$$

$$\mathbf{R}(\varphi) \equiv \left(\mathbf{r}^{k+1}, \mathbf{A}^{k+1}\varphi\right).$$

Especially, the time step size Δt in (13) is determined by setting the Courant–Friedrichs–Lewy (CFL) number to less than one. The CFL number C_{CFL} is defined as follows:

$$C_{\mathrm{CFL}} = \max\left(\frac{\Delta t\sqrt{\left(V^1\right)^2 + \left(V^2\right)^2 + \left(V^3\right)^2}}{h_{\mathrm{MESH}}}\right), \tag{14}$$

where h_{MESH} denotes the length of element.

3 Inner-front creation algorithm and optimization formulation

3.1 Procedure of inner-front creation

As mentioned earlier, in the conventional level set-based topology optimization, there exists a drawback related to the incapability of creating new inner-fronts. In this regard, the converged solution is heavily dependent on the initial level set distribution and is liable to be deviated from the optimum solution. As a motivating example, the optimization results of the conventional level set-based topology optimization method for the compliance minimization problem are represented in Fig. 3. As shown in Fig. 3, it is not allowed to create new inner-fronts in the design domain. Furthermore, it is observed that the optimum topologies depend strongly on the initial level sets.

In the present work, to overcome the shortcomings, level set-based topology optimization using an inner-front creation algorithm is proposed. A main focus of the present work is that the inner-front creation map is constructed by identifying the level value of the inner-front creation criterion concurrently considering the occupied volume (V_{OCP}) of material domain. Thus, applying the inner-front creation map to the inner-front creation process, not only positions and number of inner-fronts but also the suitable sizes of inner-fronts, can be globally and consistently identified. Especially, the criterion of inner-front creation for compliance minimization problem of a linear elastic structure is chosen as the strain energy density that corresponds to a specific case of generalized energy density. To describe the concept of generalized energy density, the following objective functional that can be written as an integral form for an arbitrary time τ is considered.

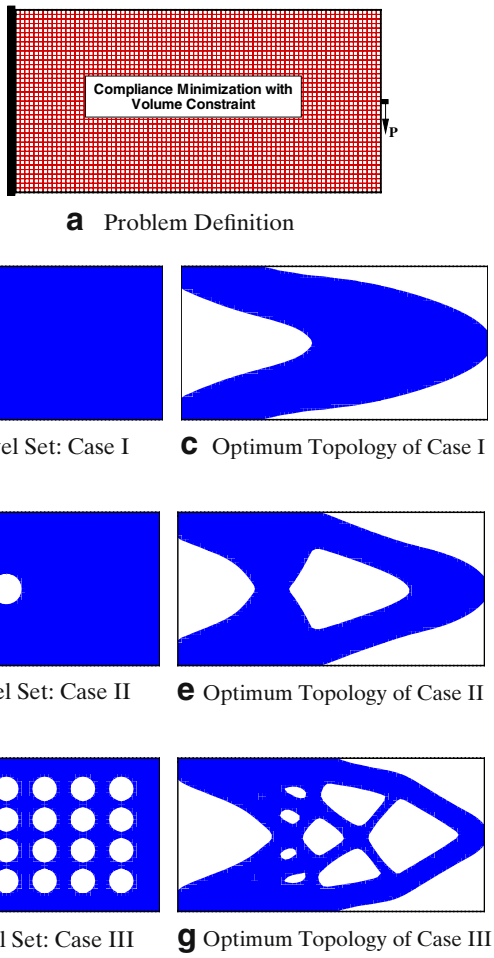

a Problem Definition

b Initial Level Set: Case I **c** Optimum Topology of Case I

d Initial Level Set: Case II **e** Optimum Topology of Case II

f Initial Level Set: Case III **g** Optimum Topology of Case III

Fig. 3 Motivating example: incapability of inner-front creation and dependency of initial level sets

$$\Psi = \int_{\Omega_\tau} g(z_\tau) d\Omega_\tau, \tag{15}$$

where Ψ is the objective functional, $z \in \mathbf{H}^1(\Omega)$ the state variable, and g the continuously differentiable function with respect to its arguments.

Considering the dependence of the functional Ψ on its domain integration and the following variational equation,

$$a\left(z_\tau, \bar{z}_\tau\right) \equiv \int_{\Omega_\tau} \theta\left(z_\tau, \bar{z}_\tau\right) d\Omega_\tau = \int_{\Omega_\tau} f\bar{z}_\tau d\Omega_\tau \equiv l_{\Omega_\tau}\left(\bar{z}_\tau\right) \quad \text{for all } \bar{z}_\tau \in Z_\tau, \tag{16}$$

where $Z_\tau \subset \mathbf{H}^m(\Omega_\tau)$ is the admissible space, $\theta(\bullet, \bullet)$ the bilinear mapping, which is defined by the integrand of

the variational equation, and f the prescribed data. From the definitions of partial derivative z' and material derivative of a domain functional (Haug et al. 1986), a variation of the functional (15) can be expressed as follows:

$$\begin{aligned}\Psi' &= \int_\Omega g_z z' d\Omega + \int_\Gamma f\left(\mathbf{V}^T\mathbf{n}\right) d\Gamma, \\ &= \int_\Omega \left[g_z \dot{z} - g_z\left(\nabla z^T \mathbf{V}\right)\right] d\Omega + \int_\Gamma f\left(\mathbf{V}^T\mathbf{n}\right) d\Gamma, \end{aligned} \tag{17}$$

where $\mathbf{V}$ denotes the shape velocity field.
By introducing the adjoint variable $z^* \in Z$, the first term in the last expression of (17), can be represented as follows:

$$\int_\Omega g_z \dot{z} d\Omega = l'(z^*) - a'\left(z, z^*\right). \tag{18}$$

Using (18) and the divergence theorem, (17) can be simply rewritten as follows:

$$\begin{aligned}\Psi' &= \int_\Gamma \left\{\theta\left(z, z^*\right) - f z^* - g_z z\right\}\left(\mathbf{V}^T\mathbf{n}\right) d\Gamma, \\ &= \int_\Gamma \Pi\left(z, z^*\right)\left(\mathbf{V}^T\mathbf{n}\right) d\Gamma, \\ &= \int_\Omega \nabla \cdot \left\{\Pi\left(z, z^*\right)\mathbf{V}\right\} d\Omega, \end{aligned} \tag{19}$$

where $\Pi\left(z, z^*\right) = \theta\left(z, z^*\right) - f z^* - g_z z$.

Π is the *generalized energy density*, as it can be derived as a form of energy density. In addition, the velocity field $\mathbf{V}$ is chosen in the direction which the objective functional should be minimized or maximized. Since this result is derived from the general objective functional, for optimization problem with different physical principles, the generalized energy density concept can also easily be devised by employing the same energy functional concept. For a more specific explanation, let us consider the compliance minimization problem subjected to the volume constraint. In the compliance minimization, the objective functional Ψ is defined as follows:

$$\Psi = \int_\Omega \mathbf{b}^T\mathbf{z} + \int_{\Gamma_{\mathrm{TRAC}}} \mathbf{t}^T\mathbf{z} d\Gamma. \tag{20}$$

where $\mathbf{b}$ is the body force, $\mathbf{t}$ the traction, Γ_{TRAC} the traction boundary, and V_{MAX} the allowable volume. As described earlier, using an adjoint variable $\mathbf{z}^*$, one can define the following functional.

$$\begin{aligned}\Psi\left(\mathbf{z}, \mathbf{z}^*\right) = &\int_\Omega \mathbf{b}^T\mathbf{z} d\Omega + \int_{\Gamma_{\mathrm{TRAC}}} \mathbf{t}^T\mathbf{z} d\Gamma - \int_\Omega \sigma(\mathbf{z})^T \varepsilon\left(\mathbf{z}^*\right) d\Omega \\ &+ \int_\Omega \mathbf{b}^T\mathbf{z}^* d\Omega + \int_{\Gamma_{\mathrm{TRAC}}} \mathbf{t}^T\mathbf{z}^* d\Gamma. \end{aligned} \tag{21}$$

Furthermore, the material derivative of (21) in the direction of $\mathbf{V}$ can be obtained as follows:

$$\begin{aligned}&\Psi'\left(\mathbf{z}, \mathbf{z}^*\right) \\ &= \int_\Omega \nabla \cdot \left[\mathbf{b}^T(\mathbf{z}+\mathbf{z}^*) - \sigma(\mathbf{z})^T \varepsilon\left(\mathbf{z}^*\right)\right] d\Omega \\ &\quad + \int_{\Gamma_{\mathrm{TRAC}}} \left[\mathbf{t}^T \nabla\left(\mathbf{z}+\mathbf{z}^*\right)^T \mathbf{n} + \kappa \mathbf{t}^T\left(\mathbf{z}+\mathbf{z}^*\right)\right] \mathbf{V}^T\mathbf{n} d\Gamma, \\ &= \int_\Omega \nabla \cdot \Big[\Big\{\mathbf{b}^T(\mathbf{z}+\mathbf{z}^*) + \mathbf{t}^T \nabla(\mathbf{z}+\mathbf{z}^*)^T\mathbf{n} \\ &\qquad + \kappa \mathbf{t}^T(\mathbf{z}+\mathbf{z}^*) - \sigma(\mathbf{z})^T \varepsilon\left(\mathbf{z}^*\right)\Big\} \mathbf{V}\Big] d\Omega, \\ &= \int_\Omega \nabla \cdot \left\{\Pi\left(\mathbf{z}, \mathbf{z}^*\right)\mathbf{V}\right\} d\Omega, \end{aligned} \tag{22}$$

where $\Pi\left(\mathbf{z}, \mathbf{z}^*\right) = \mathbf{b}^T(\mathbf{z}+\mathbf{z}^*) + \mathbf{t}^T \nabla(\mathbf{z}+\mathbf{z}^*)^T\mathbf{n} + \kappa \mathbf{t}^T(\mathbf{z}+\mathbf{z}^*) - \sigma(\mathbf{z})^T \varepsilon\left(\mathbf{z}^*\right)$.

In case of the compliance minimization problem of a linear elastic structure, the adjoint variable is simply $\mathbf{z}^* = -\mathbf{z}$; thus, $\Pi\left(\mathbf{z}, \mathbf{z}^*\right)$ in (22) is equal to the strain energy density, $\Pi\left(\mathbf{z}, \mathbf{z}\right) = \sigma(\mathbf{z})^T \varepsilon(\mathbf{z})$. Furthermore, it is noted that the topological derivative for the compliance minimization problem of a linear elastic structure can be expressed some constant times of strain energy density (Céa et al. 2000; Mei and Wang 2004; Allaire et al. 2005). Therefore, in the present work, the strain energy density is chosen as the criterion to identify the suitable positions of inner-front creation.

The success of the compliance minimization problem is closely related to the efficient use of the limited material. In this respect, the region with lower-valued strain energy density can be regarded as being underutilized, and thus, they will become the possible sites of inner-front creation. If a suitable cut-off criterion is introduced, the regions of lower-valued strain energy density can be identified. In the present work, based on the notion underlying the material usage, the occupied volume of current material domain is set as the cut-off criterion. For practical use, the distribution of strain energy density is modified to the discrete valued function, which is called inner-front creation map. The construction of inner-front creation map is described in the following. For a certain value of normalized strain energy density $\widehat{\mathrm{SE}}^*$, the discrete valued function $\chi(x)$ is defined as follows:

$$\chi(\mathbf{x}) = \begin{cases} 0 & \text{if} \quad \widehat{\mathrm{SE}}(\mathbf{x}) < \widehat{\mathrm{SE}}^*, \quad \mathbf{x} \in \Omega_{\mathrm{DES}}, \\ 1 & \text{if} \quad \widehat{\mathrm{SE}}(\mathbf{x}) \geq \widehat{\mathrm{SE}}^*, \quad \mathbf{x} \in \Omega_{\mathrm{DES}}, \end{cases} \tag{23}$$

where $\widehat{\mathrm{SE}}(\mathbf{x}) = \frac{\mathrm{SE}(\mathbf{x})}{\mathrm{SE}_{\mathrm{MAX}}}$ is the normalized strain energy density, $\mathrm{SE}(\mathbf{x})$ the strain energy density, and $\mathrm{SE}_{\mathrm{MAX}}$ the maximum strain energy density.

The domain integral of the function $\chi(\mathbf{x})$, which will be denoted $V_{\widehat{\mathrm{SE}}^*}$, is represented as follows:

$$V_{\widehat{\mathrm{SE}}^*} \equiv \int_{\Omega_{\mathrm{DES}}} \chi(\mathbf{x}) d\Omega. \tag{24}$$

For the strain energy density $\widehat{\mathrm{SE}}^*$ that satisfies $V_{\widehat{\mathrm{SE}}^*} = V_{\mathrm{OCP}}$, the inner-front creation map $H_{\mathrm{MAP}}(\mathbf{x})$ can be constructed as follows:

$$H_{\mathrm{MAP}}(\mathbf{x}) = \begin{cases} -1 \text{ for } \widehat{\mathrm{SE}}(\mathbf{x}) < \widehat{\mathrm{SE}}^*, & \mathbf{x} \in \Omega_{\mathrm{DES}}, \\ +1 \text{ for } \widehat{\mathrm{SE}}(\mathbf{x}) \geq \widehat{\mathrm{SE}}^*, & \mathbf{x} \in \Omega_{\mathrm{DES}}. \end{cases} \tag{25}$$

The construction procedure of inner-front creation map is illustrated in Fig. 4.

In the implementation of inner-front creation algorithm, the updated level set function with new inner-fronts can be generated by multiplying the current level set function, inner-front creation map, and sign function. Namely,

$$\phi^{\mathrm{NEW}}(\mathbf{x}) = \mathrm{Sgn}(\mathbf{x}) \circ H_{\mathrm{MAP}}(\mathbf{x}) \circ \phi^{\mathrm{OLD}}(\mathbf{x}), \quad \mathbf{x} \in \Omega_{\mathrm{DES}}, \tag{26}$$

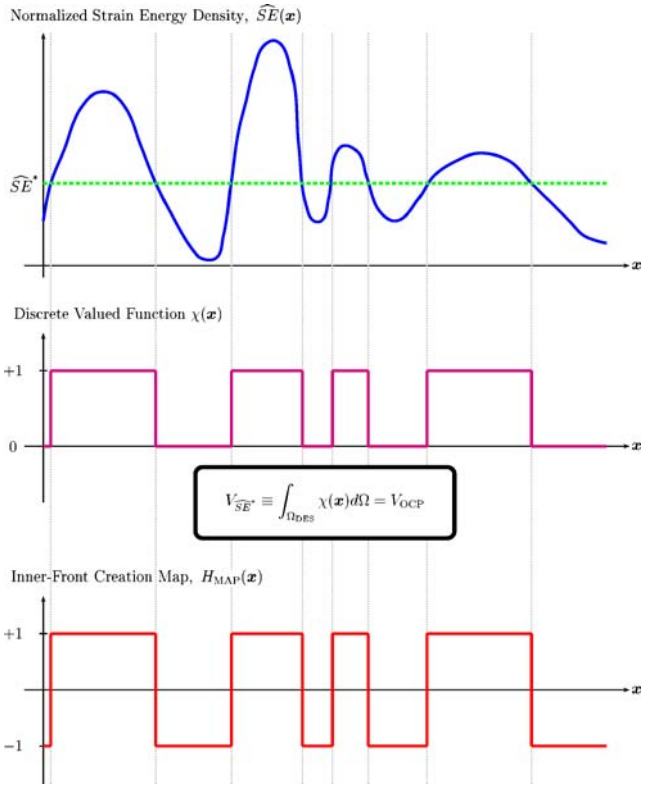

Fig. 4 Construction of inner-front creation map

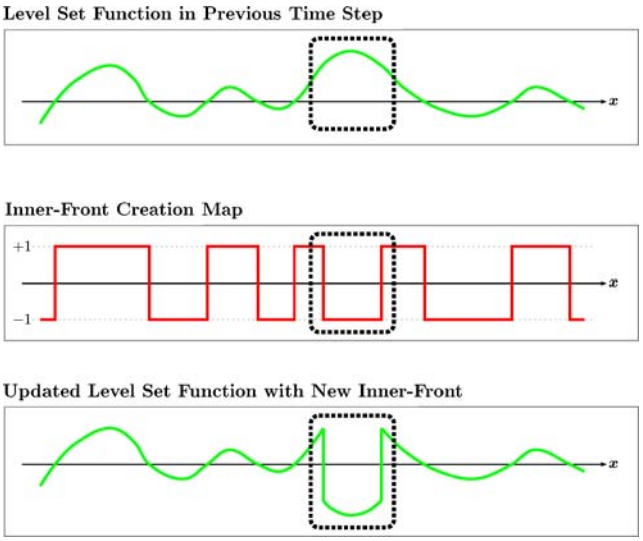

Fig. 5 Schematic diagram of inner-front creation process

where

$$\mathrm{Sgn}(\mathbf{x}) = \begin{cases} -1 & \text{for } \phi^{\mathrm{OLD}}(\mathbf{x}) < 0 \text{ and } H_{\mathrm{MAP}}(\mathbf{x}) = -1, \\ +1 & \text{otherwise}, \end{cases}$$

is the sign function, $\circ$ the multiplication operator of two functions, i.e. $a(\mathbf{x}) \circ b(\mathbf{x}) = a(\mathbf{x}) b(\mathbf{x})$, $\phi^{\mathrm{NEW}}(\mathbf{x})$ the level set function with new inner-fronts, and $\phi^{\mathrm{OLD}}(\mathbf{x})$ the current level set function.

The overall inner-front creation process is represented in Fig. 5.

Due to the piecewise constant distribution of the inner-front creation map, the sharp edges in the level set function possessing new inner-fronts are appeared. Since these sharp edges may adversely affect the convergence speed and/or numerical stability, the edge smoothing process is required. In the present work, to make isotropic linear Gaussian filtering effects on the level set function possessing sharp edges, the smoothing PDE that is widely used in the image processing is adopted. The edge smoothing PDE is expressed as the following linear parabolic equation:

$$\frac{\partial \phi}{\partial \eta} - \nabla^2 \phi = 0, \tag{27}$$

with initial condition:

$$\phi(\mathbf{x}, \eta = \eta_0) = \phi_0(\mathbf{x}),$$

where η denotes the pseudo-time that acts as the time variable of edge smoothing PDE.

In the computation of (27), standard Galerkin finite element method with the backward difference approximation in time is employed. That is,

$$\int_\Omega \phi^{m+1}\omega d\Omega - \Delta\eta \int_\Omega \nabla\phi^{m+1}\cdot\nabla\omega d\Omega = \int_\Omega \phi^m \omega d\Omega \quad \text{for all } \omega \in \mathbf{H}^1(\Omega), \tag{28}$$

where m is the m-th time step and $\Delta\eta = \eta^{m+1} - \eta^m$ the time step size.

In the present work, since the purpose of edge smoothing is to obtain level set function with smooth boundaries that enable the numerical oscillation to be avoided during the optimization process, considering the computational time, the level set function with new inner-fronts is updated only twice in the edge smoothing process. The smoothing effect on the level set function with sharp edges is illustrated in Fig. 6.

3.2 Formulation of compliance minimization problem

In this section, the optimization formulation and the shape sensitivity analysis for compliance minimization problem of a linear elastic shell structure subjected to the volume constraint are outlined. The detailed descriptions of overall optimization formulation can be found at Sethian and Wiegmann (2000), Wang et al. (2003), and Allaire et al. (2004). Especially, as for the shape sensitivity analysis, Simon (1980), Haug et al. (1986), and Haftka and Gürdal (1992) provide a well-established theoretical background.

The linear elastic problem to analyze static responses of the shell structure is described as follows:

$$\nabla\cdot\sigma = -\mathbf{f} \quad \text{in } \Omega_{\text{DES}}, \tag{29a}$$

$$\mathbf{u} = \mathbf{g} \quad \text{on } \Gamma_{\text{DISP}}, \tag{29b}$$

$$\sigma^T\mathbf{n} = \mathbf{h} \quad \text{on } \Gamma_{\text{TRAC}}, \tag{29c}$$

where Γ_{DISP} and Γ_{TRAC} are the boundaries, respectively, of the design domain on which the essential boundary condition and the natural boundary condition are imposed, $\mathbf{u}$ the displacement vector, $\sigma = \mathbf{E}\varepsilon$ the stress vector, $\mathbf{E}$ the elasticity matrix, ε the strain vector, $\mathbf{n}$ the outer unit normal vector on Γ_{TRAC}, and $\mathbf{f}$, $\mathbf{g}$, and $\mathbf{h}$ the prescribed data on Ω_{DES}, Γ_{DISP}, and Γ_{TRAC}, respectively.

By applying the Galerkin method and embedding the level set function ϕ to (29a)–(29c), the following variational formulation can be constructed:

$$\mathbf{a}_\phi(\mathbf{u},\mathbf{v}) = \mathbf{l}_\phi(\mathbf{v}) \quad \text{for all } \mathbf{v} \in \mathbf{H}^1(\Omega), \tag{30}$$

where

$$\mathbf{a}_\phi(\mathbf{u},\mathbf{v}) = \int_{\Omega_{\text{DES}}} H(\phi)\varepsilon_{\mathbf{u}}^T\mathbf{E}\varepsilon_{\mathbf{v}}d\Omega,$$

$$l_\phi(\mathbf{v}) = \int_{\Gamma_{\text{TRAC}}} H(\phi)\mathbf{h}^T\mathbf{v}d\Gamma + \int_{\Omega_{\text{DES}}} H(\phi)\mathbf{f}^T v d\Omega,$$

and $\varepsilon_{\mathbf{u}} = \frac{\nabla\mathbf{u}+\nabla\mathbf{u}^T}{2}$ is the stain vector with respect to its argument displacement $\mathbf{u}$.

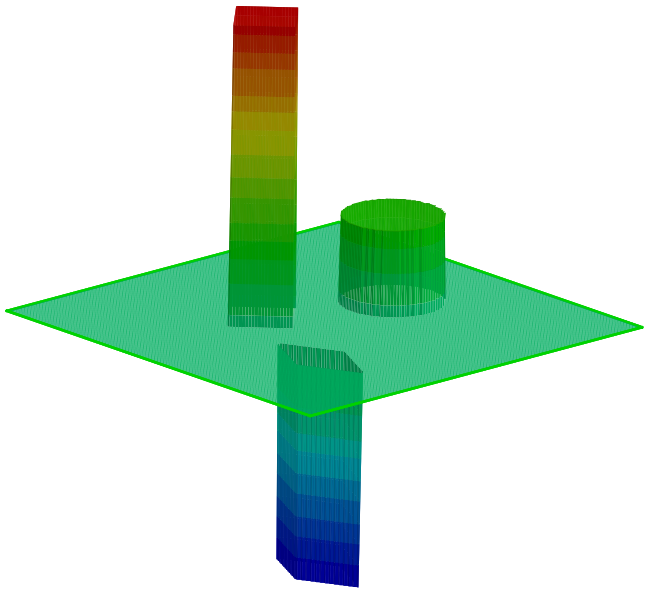

a Level Set Function with Sharp Edges

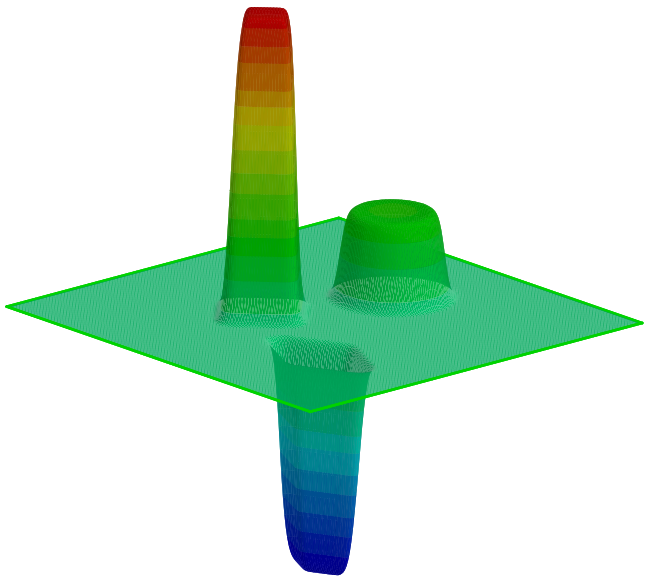

b Level Set Function with Smooth Edges

Fig. 6 Effect of edge smoothing via smoothing PDE

Based on the general framework of optimization formulation, the compliance minimization problem subjected to the volume constraint can be stated as follows:

$$\begin{aligned}\text{Minimize} \quad \mathcal{F}_{\text{COMP}}(\mathbf{u},\phi) &\equiv \int_{\Omega_{\text{DES}}} H(\phi)\varepsilon_{\mathbf{u}}^T \mathbf{E}\varepsilon_{\mathbf{u}} d\Omega \\ &= \int_{\Gamma_{\text{TRAC}}} H(\phi)\mathbf{h}^T\mathbf{u} d\Gamma \\ &\quad + \int_{\Omega_{\text{DES}}} H(\phi)\mathbf{f}^T\mathbf{u} d\Omega, \end{aligned} \tag{31a}$$

$$\text{subject to} \quad \mathcal{H}_{\text{VOL}}(\phi) \equiv \int_{\Omega_{\text{DES}}} H(\phi) d\Omega - \xi_{\text{VOL}} \cdot V_{\text{TOT}} \leq 0, \tag{31b}$$

where ξ_{VOL} is the prescribed volume ratio.

Using the Lagrange multiplier, the constrained minimization problem of (31a) and (31b) can be reformulated as the following Lagrangian form:

$$\mathcal{L}(\mathbf{u},\phi,\lambda) = \int_{\Omega_{\text{DES}}} \left[H(\phi)\mathcal{U}(\mathbf{u}) + \lambda\left(H(\phi) - \xi_{\text{VOL}}\right)\right] d\Omega, \tag{32}$$

where $\mathcal{L}(\mathbf{u},\phi,\lambda)$ is the Lagrangian functional, λ the Lagrange multiplier, and $\mathcal{U}(\mathbf{u}) = \varepsilon_{\mathbf{u}}^T \mathbf{E}\varepsilon_{\mathbf{u}}$.

In the present work, the Lagrangian functional in (32) is considered in the optimization procedure.

3.2.1 Shape design sensitivity analysis

To define the shape design sensitivity, it is convenient to consider the concept of original and perturbed domain as a continuous medium. The process of deforming reference domain Ω_0 and perturbed domain Ω_τ by the mapping $M(\Omega_0,\tau)$ may be regarded as a dynamic process of deforming a continuum, with τ playing the role of time. In neighbor of $\tau = 0$, under a certain regularity hypothesis (Haug et al. 1986; Oden and Demkowicz 1996), $\mathbf{x}_\tau \in \Omega_\tau$ can be expressed as follows:

$$\mathbf{x}_\tau = \mathbf{x} + \tau \mathbf{V}_{\text{SV}}(\mathbf{x}). \tag{33}$$

where $\mathbf{V}_{\text{SV}}(x_\tau,\tau) \equiv \dfrac{d\mathbf{x}_\tau}{d\tau} = \dfrac{\partial M(\mathbf{x},\tau)}{\partial\tau}$ is the shape velocity.

With this context, by considering the shape velocity $\mathbf{V}_{\text{SV}}$, (2) can be modified as follows:

$$\frac{\partial\phi}{\partial t} + \mathbf{V}_{\text{SV}} \cdot \nabla\phi = 0. \tag{34}$$

In the level set-based topology optimization, (34) governs the evolution of material boundary during optimization process.

To carry out the shape design sensitivity analysis for the optimization problem in (32), let us consider the boundary variation in the direction of ψ. Then the shape derivative of the Lagrangian functional in (32) is obtained as follows:

$$\left.\frac{\partial\mathcal{L}(\mathbf{u},\phi,\lambda)}{\partial\phi}\right|_\psi = \left.\frac{\partial\mathcal{F}_{\text{COMP}}(\mathbf{u},\phi)}{\partial\mathbf{u}}\right|_\mu + \left.\frac{\partial\mathcal{F}_{\text{COMP}}(\mathbf{u},\phi)}{\partial\phi}\right|_\psi + \lambda \left.\frac{\partial\mathcal{H}_{\text{VOL}}(\phi)}{\partial\phi}\right|_\psi, \tag{35}$$

where $\left.\dfrac{\partial\mathcal{L}(\mathbf{u},\phi,\lambda)}{\partial\phi}\right|_\psi = \displaystyle\int_{\Omega_0} \frac{\partial\mathcal{L}(\mathbf{u},\phi,\lambda)}{\partial\phi}\psi d\Omega$ is the Fréchet derivative of Lagrangian functional with respect to ϕ in the direction of ψ, ψ the direction of shape variation, and μ the direction that is introduced to represent the implicit dependence of displacement field $\mathbf{u}$ during the shape variation of domain in the ψ-direction.

By introducing an adjoint variable $v \in \mathbf{H}^1(\Omega)$, which is employed to represent the sensitivity of the first term of (35) with respect to displacement field u as the form of level set function ϕ and the shape variation in the ψ-direction, the first term in the right-hand side of (35) is represented as follows:

$$\begin{aligned}&\left.\frac{\partial\mathcal{F}_{\text{COMP}}(\mathbf{u},\phi)}{\partial\mathbf{u}}\right|_\mu \\ &\equiv \int_{\Omega_0} \delta(\phi)\left[\mathbf{f}^T\mathbf{v} + \kappa\left\{\mathbf{h}^T\mathbf{v}\right\} - \varepsilon_{\mathbf{u}}^T\mathbf{E}\varepsilon_{\mathbf{v}}\right]\psi d\Omega \\ &\quad + \int_{\Gamma_0} \delta(\phi)\frac{\delta(\phi)}{|\nabla\phi|}\frac{\partial\phi}{\partial\mathbf{n}}\psi d\Gamma. \end{aligned} \tag{36}$$

where $\kappa = \nabla \cdot \dfrac{\nabla\phi}{|\nabla\phi|}$ denotes the curvature.

Furthermore, the second and third terms on the right-hand side of (35) are defined as follows, respectively:

$$\left.\frac{\partial\mathcal{F}_{\text{COMP}}(\mathbf{u},\phi)}{\partial\phi}\right|_\psi \equiv \int_{\Omega_0} \delta(\phi)\mathcal{U}(\mathbf{u})\psi d\Omega, \tag{37a}$$

$$\left.\frac{\partial\mathcal{H}_{\text{VOL}}(\phi)}{\partial\phi}\right|_\psi \equiv \int_{\Omega_0} \delta(\phi)\psi d\Omega. \tag{37b}$$

Incorporating the results of (36), (37a), and (37b), the shape design sensitivity of Lagrangian functional in (35) is expressed as follows:

$$\begin{aligned}
&\left.\frac{\partial \mathcal{L}(\mathbf{u},\phi,\lambda)}{\partial \phi}\right|_{\psi} \\
&= \int_{\Omega_0} \delta(\phi)\left[\mathcal{U}(\mathbf{u}) + \mathbf{f}^T\mathbf{v} + \kappa\left\{\mathbf{h}^T\mathbf{v}\right\} - \varepsilon_{\mathbf{u}}^T\mathbf{E}\varepsilon_{\mathbf{v}} + \lambda\right]\psi d\Omega \\
&\quad + \int_{\Gamma_0} \delta(\phi)\frac{\delta(\phi)}{|\nabla\phi|}\frac{\partial\phi}{\partial\mathbf{n}}\psi d\Gamma \\
&= \int_{\Omega_0} \delta(\phi)\left[\mathcal{M}_{\phi}(\mathbf{u},\mathbf{v}) + \lambda\right]\psi d\Omega \\
&\quad + \int_{\Gamma_0} \delta(\phi)\frac{\delta(\phi)}{|\nabla\phi|}\frac{\partial\phi}{\partial\mathbf{n}}\psi d\Gamma, \qquad (38)
\end{aligned}$$

where $\mathcal{M}_{\phi}(\mathbf{u},\mathbf{v}) \equiv \mathcal{U}(\mathbf{u}) + \mathbf{f}^T\mathbf{v} + \kappa\left\{\mathbf{h}^T\mathbf{v}\right\} - \varepsilon_{\mathbf{u}}^T\mathbf{E}\varepsilon_{\mathbf{v}}$.

Applying the Karush–Kuhn–Tucker condition to (32) and (38) and vanishing the boundary integration term of (38), the final form of shape design sensitivity of the Lagrangian functional can be denoted as follows:

$$\left.\frac{\partial \mathcal{L}(\mathbf{u},\phi,\lambda)}{\partial \phi}\right|_{\psi} = \int_{\Omega_0} \delta(\phi)\left[\mathcal{M}_{\phi}(\mathbf{u},\mathbf{v}) + \lambda\right]\psi d\Omega. \qquad (39)$$

3.2.2 Determination of shape velocity and Lagrange multiplier

In this section, the procedure to obtain the shape velocity from the shape design sensitivity analysis is described. Based on the concept of shape variation, the Lagrangian functional considering boundary variation at original domain is obtained as follows:

$$\mathcal{L}(\Omega_\tau) = \mathcal{L}(\Omega_0) - \tau\mathbf{V}_{\mathrm{SV}}\mathcal{L}'(\Omega_0), \qquad (40)$$

where $\mathcal{L}'(\Omega_0)$ denotes the shape design sensitivity of the Lagrangian functional at the original domain. In the present work, the shape velocity is taken as follows:

$$\mathbf{V}_{\mathrm{SV}} = \left[\mathcal{M}_{\phi}(\mathbf{u},\mathbf{v}) + \lambda\right]\psi. \qquad (41)$$

By defining the shape velocity as (41) and applying it to (40), the decrease of the Lagrangian functional is ensured as follows:

$$\mathcal{L}(\Omega_\tau) = \mathcal{L}(\Omega_0) - \tau\int_{\Omega_0} \delta(\phi)\left[\{\mathcal{M}_{\phi}(\mathbf{u},\mathbf{v}) + \lambda\}\psi\right]^2 d\Omega, \qquad (42)$$

Therefore, based on the mathematical framework for the shape design sensitivity analysis, the level set-based topology optimization method satisfying the decrease of objective function can be obtained.

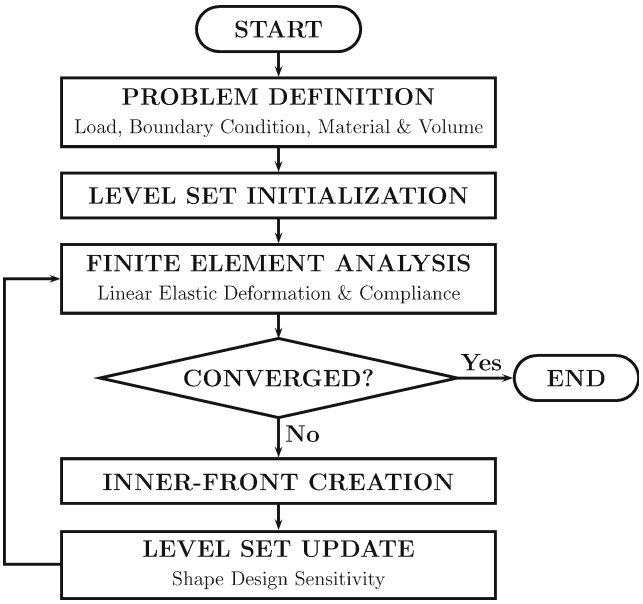

Fig. 7 Flowchart of overall optimization procedure

To update the Lagrange multiplier λ, Rosen's (1960) approach is adopted in the present work. By taking time derivative of active constraint of (31b) and using (34) and (41), the following equation is obtained:

$$\begin{aligned}
\frac{\partial}{\partial t}\left[\int_{\Omega_0} H(\phi)d\Omega\right] &= \int_{\Omega_0} \delta(\phi)\mathbf{V}_{\mathrm{SV}}\cdot\nabla\phi d\Omega, \\
&= \int_{\Omega_0} \delta(\phi)\left[\mathcal{M}_{\phi}(\mathbf{u},\mathbf{v}) + \lambda\right]\psi\cdot\nabla\phi d\Omega, \\
&= 0. \qquad (43)
\end{aligned}$$

Therefore, the Lagrange multiplier can be computed from the following equation:

$$\lambda = -\frac{\displaystyle\int_{\Omega_0} \delta(\phi)\mathcal{M}_{\phi}(\mathbf{u},\mathbf{v})\psi\cdot\nabla\phi d\Omega}{\displaystyle\int_{\Omega_0} \delta(\phi)\psi\cdot\nabla\phi d\Omega}. \qquad (44)$$

Table 1 Problem definition for design of cantilever beam

Parameter	Specified data
Geometry	$W = 2$ m, $H = 1$ m, $L_T = 1$ cm
Mesh	3,200 (80 by 40) Linear quadrilateral shell element
Material	Steel (Young's modulus $E = 200$ GPa, Poisson's ratio $\nu = 0.3$)
Volume ratio	50% ($\xi_{\mathrm{VOL}} = 0.5$)
Applied load	$P = 20$ kN

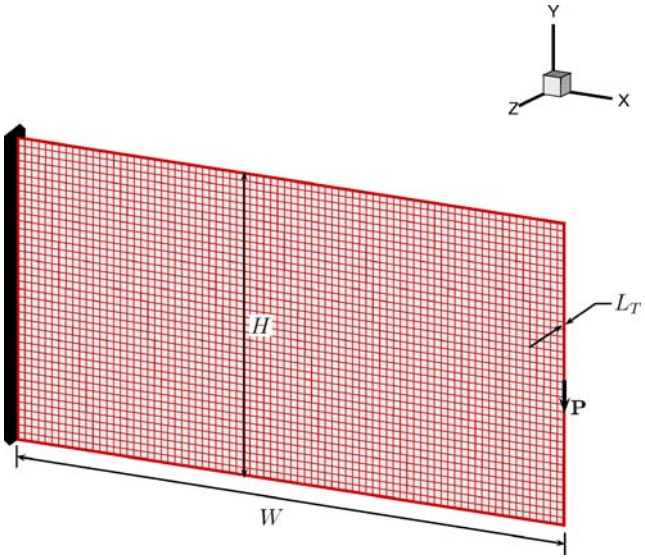

Fig. 8 Schematic diagram of cantilever beam design

4 Applications

In the present work, topology optimization of shell structures using the adaptive inner-front creation level set method is treated. Although there have been shell structures since ancient times, the significant progress in research for topology and shape optimization has been made only recently in conjunction with the rapid development of powerful methodologies such as finite element methods. Tenek and Hagiwara (1994) has developed a scheme for determining thickness distribution or the density of a repetitious microstructure using homogenization theory. Maute and Ramm (1996) have solved the maximum stiffness problems for shell structures by combining the adaptive optimization technique with the homogenization concept. Li et al. (1999) has applied the evolutionary structural optimization to the topology optimization of shell structures subjected to thermal loading. The shell stiffener and core layout design have been treated by Lee et al. (2000) and Belblidia and Bulman (2002). To the best of our knowledge, no work before the present work applies level set method to topology optimization of shell structures.

In the applications, in the present work, three-dimensional linear elastic shell structures are considered. Based on the Reissner–Mindlin shell theory permitting the transverse shear deformation, general curved shell structures are dealt with. To avoid the element locking, in the present work, the selective reduced integration is employed. The membrane locking is not considered, as the shell thicknesses were regarded as being relatively thick.

The optimization problem is given as the compliance minimization subjected to volume constraint. Especially, the following three applications—design of cantilever beam, doubly curved shell, and lightweight steel deck—are dealt with. The overall procedure of level set-based topology optimization using inner-front creation map is shown in Fig. 7. The optimization process is summarized as follows: At first, the

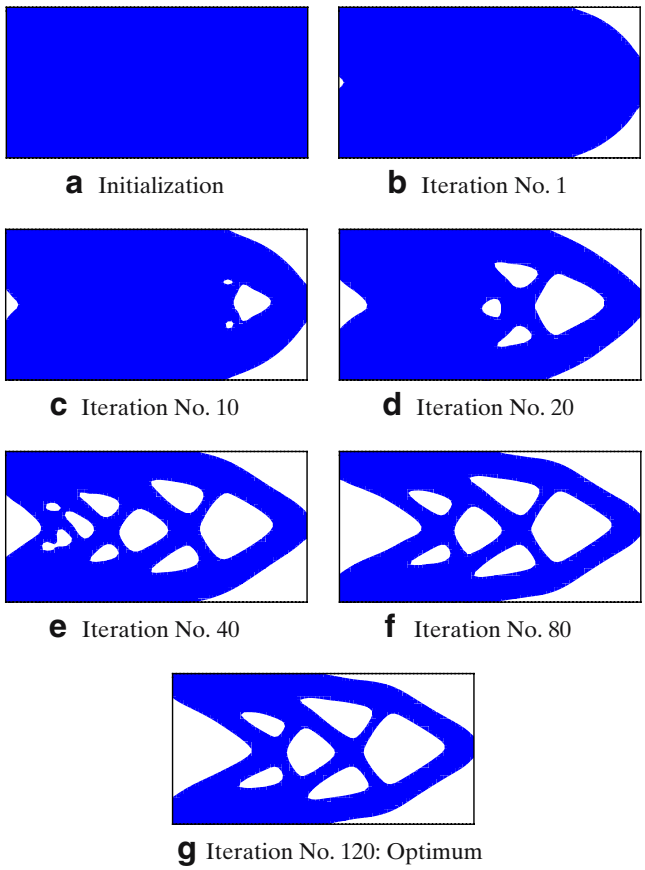

Fig. 9 History of optimization for cantilever beam

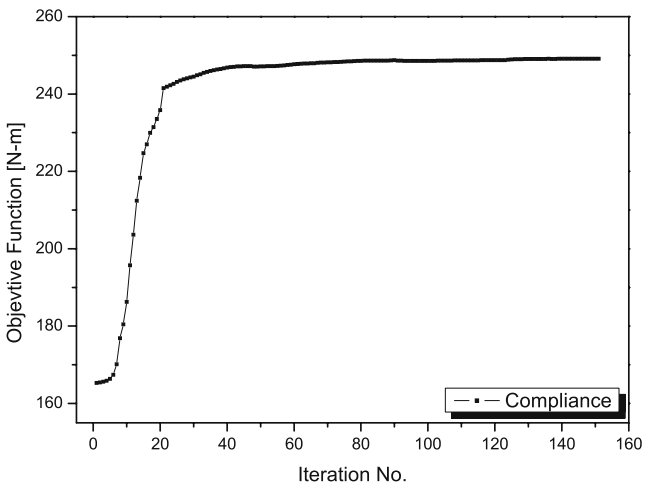

Fig. 10 History of objective function for cantilever beam design

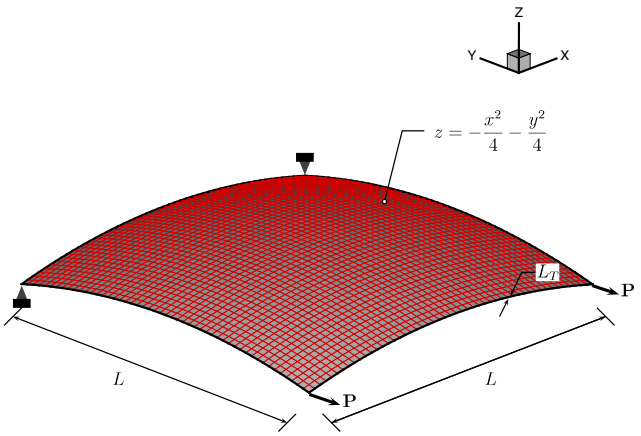

Fig. 11 Schematic diagram of doubly curved shell design

optimization problem including load, boundary condition, and constraint volume is imposed. And then, initial level set function is defined on the design domain of a structure. Via the finite element analysis, the elastic deformation, compliance, and strain energy density are computed. Employing the inner-front creation map, which is constructed from the strain energy density value, the inner-front creation process is performed. In addition, to smooth out the sharp edges of the level set function with new inner-fronts, the edge smoothing process is carried out. By solving the level set equation employing the shape velocity, which is obtained from the shape sensitivity analysis, the level set function and design domain are updated. Until the objective function converges, the finite element analysis, inner-front creation, and level set update are repeated.

4.1 Example 1: cantilever beam

As a standard example, cantilever beam that is widely treated in the conventional topology optimization method is considered. The design domain is set as 2 by 1 m rectangular shape. To discretize the design domain, four-node linear shell elements are employed. As the constraint, the volume ratio of optimum topology is limited to 50%. A concentrated load of 20 kN is applied at the center of the right-hand side of the design domain. The design conditions are summarized in Table 1. The schematic diagram of the design problem is shown in Fig. 8. The initial level set is distributed on whole design domain. To demonstrate the aspects of inner-front creation, the evolutionary history of material boundary at certain iterations is represented in Fig. 9. As shown in the last result of Fig. 9, the proposed method can handle the changes of shape and topology at the same

Table 2 Problem definition for design of doubly curved shell structure

Parameter	Specified data
Geometry	L =1 m, L_T =1 cm
Mesh	2,500 (50 by 50) Linear quadrilateral shell element
Material	Steel (E = 200 GPa, ν =0.3)
Volume ratio	50% (ξ_{VOL} =0.3)
Applied load	P = 1 kN

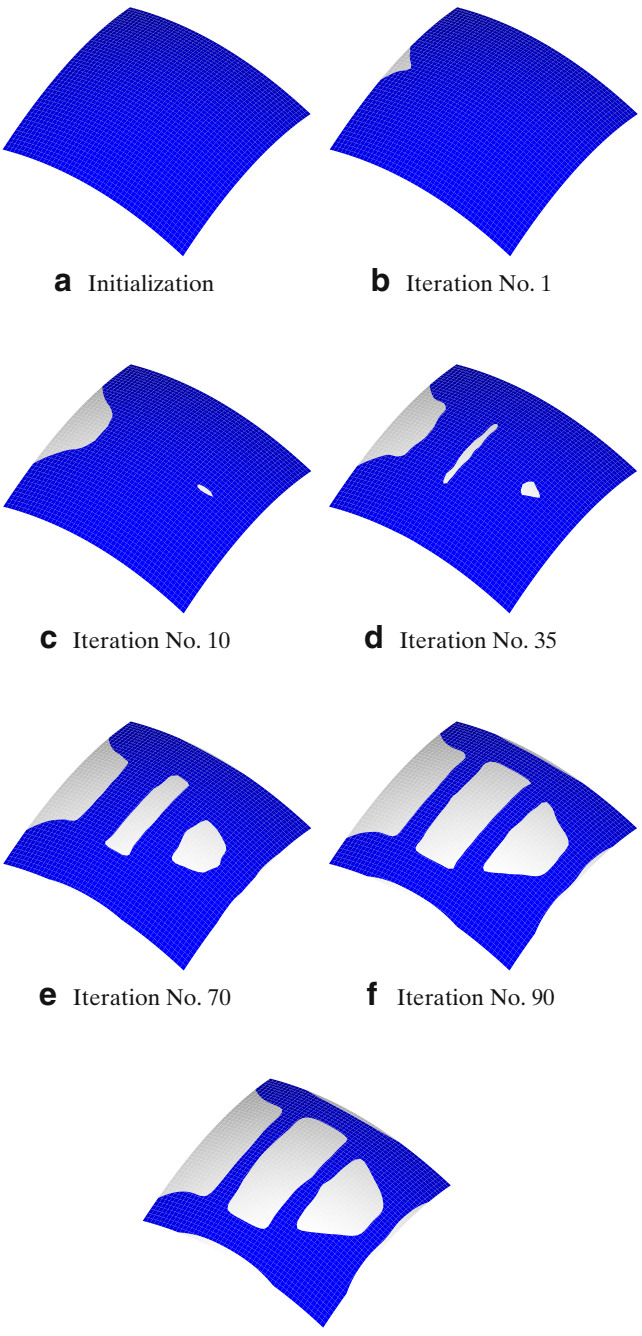

Fig. 12 History of optimization for doubly curved shell structure

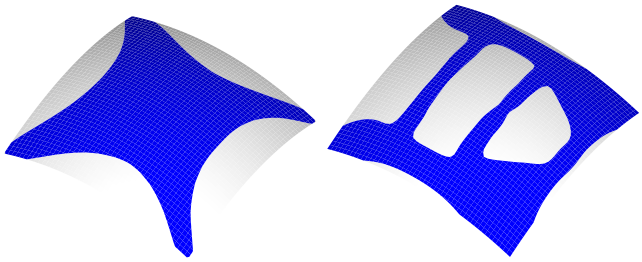

Fig. 13 Comparison of optimum topology between proposed and conventional approaches

Table 3 Problem definition for design of lightweight steel deck

Parameter	Specified data
Geometry	$L = 1.2$ m, $L_S = 20$ cm, $L_H = 11$ cm, $L_T = 1$ mm
Mesh	2, 500 (50 by 50) Linear quadrilateral shell element
Material	Steel ($E = 200$ GPa, $\nu = 0.3$)
Volume ratio	30% ($\xi_{\mathrm{VOL}} = 0.3$)
Applied load	$P_1 = 10$ kN, $P_2 = 20$ kN, $P_3 = 1$ kN

time. The history of objective function is represented in Fig. 10. As shown in Fig. 10, as the volume constraint is not satisfied at the early stage of optimization, the objective function is increased. However, once the volume constraint is satisfied, the objective function is monotonically converged to a certain value.

4.2 Example 2 : doubly curved shell structure

As the second example, topology optimization of doubly curved shell structure is carried out. This is a design example of the stiffened panel for a roof structure that supports two concentric edge loads. A 1 by 1 m curved square is considered as the design domain. The volume constraint of the optimization problem is set to 50%. The schematic diagram of the design problem is shown in Fig. 11. As shown in Fig. 11, two concentric loads are imposed at both edges of the curved shell. The design conditions are summarized in Table 2. As the same initialization, the level set is distributed on the whole design domain. The histories of level set at certain iterations are represented in Fig. 12. In Fig. 12, new inner-fronts with smooth boundaries are created at iteration no. 10 and iteration no. 35, and then, the inner-fronts are widened during the optimization process. In addition, from Fig. 12, it is observed that the inner-front creation algorithm can provide the shapes, positions, and number of inner-fronts at once. Figure 13 represents optimum topology obtained from the present and conventional methods. In Fig. 13, it is shown that the proposed method can accomplish the shape and topology changes bringing the inner-front creation. The history of objective function is represented in Fig. 14. As shown in Fig. 14, although the objective function is increased at several iterations, the objective functional value is converged to a certain value.

4.3 Example 3: lightweight steel deck design

As an extended example, the lightweight steel deck that is used for providing longer span for floor construction is carried out. Among other influences, in the conventional design of the steel deck, the stiffness

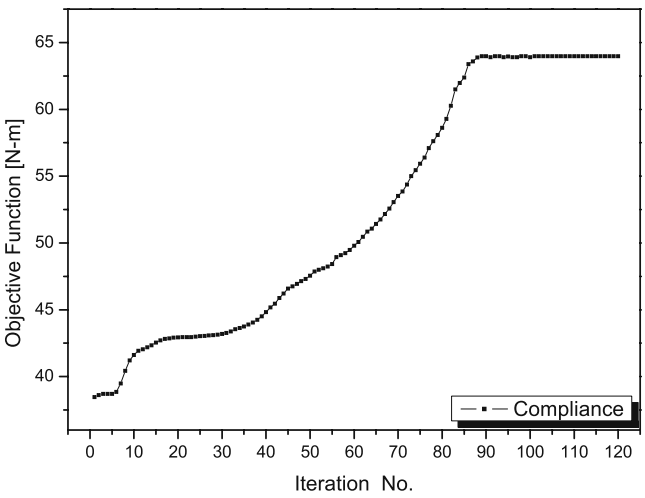

Fig. 14 History of objective function for doubly curved shell structure

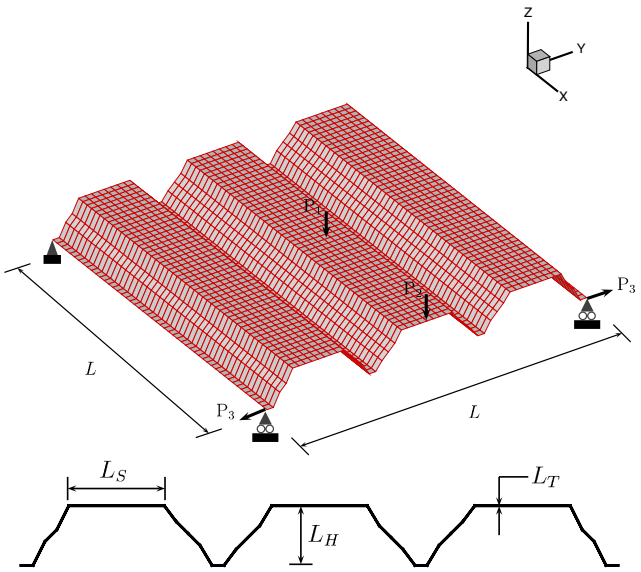

Fig. 15 Schematic diagram of lightweight steel deck design

of the deck is determined by shear force traveling in the hat-shaped (curved) directions. Furthermore, the hat-shaped elements have tendency to warp and/or roll over in shear. With flexibility and with shear warping in the hat shape, the steel deck should resist even more of the applied load. In addition, due to the handling limitation and manufacturing cost, total weight of the steel deck should be kept low. In the present work, topology optimization of lightweight steel deck is carried out. The design conditions are summarized in Table 3. The schematic diagram of the design problem is shown in Fig. 15. The initial level set is distributed on the whole design domain. To demonstrate the aspects of inner-front creation, the evolutionary history of material boundary at certain iterations is represented in Fig. 16. In Fig. 16, it can be observed that an optimum structure to resist and to minimize the deformation in the hat-shaped direction is obtained. Furthermore, at iteration no. 10, an inner-front is created near the position of applied load P_1. In Fig. 17, the optimum topology of proposed and conventional approaches is illustrated. As represented in Fig. 17, compared with the conventional approach, it is shown that the present method brings in much flexible topological changes. The history of objective function is represented in Fig. 18. As shown in Fig. 18, although the objective function possesses certain bumps, finally, it converges monotonically.

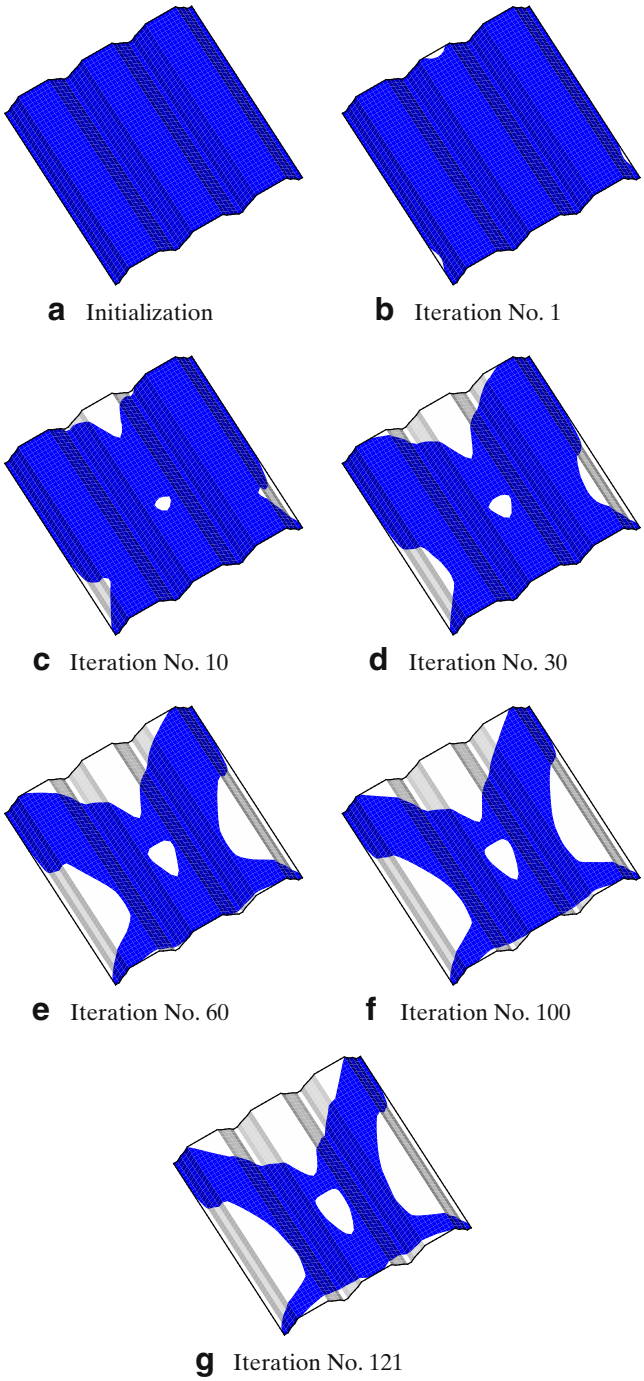

Fig. 16 History of optimization for lightweight steel deck

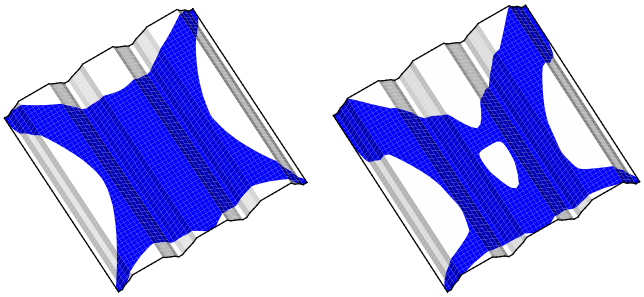

Fig. 17 Comparison of optimum topology between proposed and conventional approaches

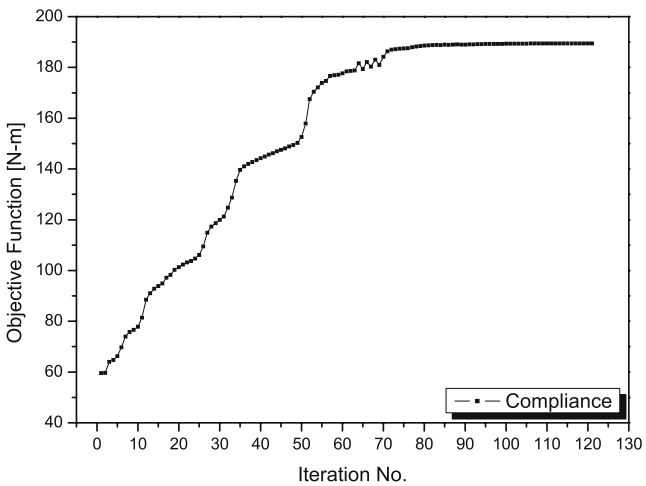

Fig. 18 History of objective function for lightweight steel deck

5 Conclusions

In the present work, a new level set-based topology optimization using inner-front creation algorithm is proposed. Based on the given inner-front creation criterion, to identify the sizes and positions of inner-fronts globally and consistently, the occupied volume of material domain is utilized. To facilitate the inner-front creation process, the inner-front creation map, which corresponds to the discrete valued criterion of inner-front creation, is applied to the level set function. As an inner-front creation criterion, the strain energy density, which is, in a sense, a generalized energy density for compliance minimization problem of linear elastic structure, is employed.

In the implementation of inner-front creation algorithm, to suppress the numerical oscillation of solutions due to the sharp edges in the level set function, the edge smoothing is carried out by solving the edge smoothing PDE.

Based on the general framework of shape design sensitivity analysis, the shape velocity that is used as the velocity term of the level set equation is computed. To update the level set function, the LSFEM is adopted. Through the LSFEM, a symmetric positive definite system matrix is constructed, and non-diffused and non-oscillatory solution for level set equation can be obtained.

For applications, topology optimizations of shell structures are presented and illustrated. In the numerical examples, it is shown that creation of new inner-fronts in the design domain are occurred. As the results, the evolution of level set function and the history of objective function have been illustrated and discussed. From the results, it is observed that the present method brings in much needed flexibility in topologies during the level set-based topology optimization process.

References

Allaire G, Jouve F, Toader AM (2004) Structural optimization using sensitivity analysis and a level set method. J Comput Phys 194:363–393

Allaire G, Jouve F, Toader AM (2005) Structural optimization using topological and shape sensitivity via a level set method. Control Cyber 34:59–80

Amstutz V, Andra H (2006) A new algorithm for topology optimization using a level-set method. J Comput Phys 216: 573–588

Aubert G, Kornprobst P (2001) Mathematical problems in image processing: partial differential equations and the calculus of variations. Springer, Berlin

Belblidia F, Bulman S (2002) A hybrid topology optimization algorithm for static and vibrating shell structures. Int J Numer Methods Eng 54:835–852

Bendsøe MP, Kikuchi N (1988) Generating optimal topologies in structural design using a homogenization method. Comput Methods Appl Mech Eng 71:197–224

Bendsøe MP, Sigmund O (2003) Topology optimization—theory, methods and applications. Springer-Verlag, Berlin

Burger M, Hackl B, Ring W (2004) Incorporating topological derivatives into level set methods. J Comput Phys 194: 344–362

Céa J, Garreau S, Guillaume P, Masmoudi M (2000) The shape and topological optimizations connection. Comput Methods Appl Mech Eng 188:713–726

Ha SH, Cho SH (2005) Topological shape optimization of heat conduction problems using level set approach. Numer Heat Trans Part B 48:67–88

Haftka RT, Gürdal Z (1992) Elements of structural optimization. Kluwer, Dordrechet

Harber RB, Jog CS, Bendsøe MP (1996) A new approach to variable—topology shape design using a constraint on perimeter. Struct Optim 11:1–12

Haug EJ, Choi KK, Komkov V (1986) Design sensitivity analysis of structural systems. Academic, Orlando

Jiang BN (1998) The least-squares finite element method. Springer, Berlin

Kwak JH, Cho SH (2005) Topological shape optimization of geometrically nonlinear structures using level set method. Comput Struct 83:2257–2268

Lee S, Soni BK (1997) Governing equation of fluid mechanics in physical curvilinear coordinate system. In: Proceedings of the 3rd Mississippi state conference on difference equations and computational simulations. Mississippi State, USA, pp 149–157

Lee SJ, Bae JE, Hinton E (2000) Shell topology optimization using the layered artificial material model. Int J Numer Methods Eng 47:843–867

Li Q, Steven GP, Querin OM (1999) Optimization of thin shell structures subjected to thermal loading. Struct Eng Mech 7:401–412

Maute K, Ramm E (1996) Adpative topology optimization of shell structures. In: Proceedings of the 6th AIAA/ NASA/ISSMO symposium on multidisciplinary analysis and optimization. Bellevue, USA, pp 1133–1141

Mei Y, Wang XM (2004) Level set method for structural topology optimization and its applications. Adv Eng Softw 35:415–441

Novotny AA, Feijoo RA, Taroco E, Padra C (2003) Topological sensitivity analysis. Comput Methods Appl Mech Eng 192:803–829

Oden JT, Demkowicz LF (1996) Applied functional analysis. CRC Press, Florida

Osher S, Fedkiw R (2003) Level set methods and dynamic implicit surfaces. Springer, Berlin

Osher S, Sethian JA (1998) Fronts propagating with curvature dependent speed: algorithms based on Hamilton–Jacobi formulations. J Comput Phys 79:12–49

Rosen JB (1960) The gradient projection method for nonlinear programming, part I, linear constraints. J Soc Industrial Appl Math 8:181–217

Sethian JA (1999) Level set methods and fast marching methods: evolution interfaces in computational geometry, fluid mechanics, computer vision, and meterail science. Cambridge Univ. Press, Cambridge

Sethian JA, Wiegmann (2000) A structural boundary design via level se and immersed interface method. J Comput Phys 163:489–528

Simon J (1980) Differentiation with respect to the domain in boundary value problems. Numer Function Anal Optim 2:649–687

Sokołowski J, Żochowski A (1999) On the topological derivative in shape optimization. SIAM J Control Optim 37:1251–1272

Takahira H, Horiuchi T, Banerjee S(2004) An improved three-dimensional level set method for gas–liquid two-phase flows. J Fluids Eng 126:578–585

Tenek LH, Hagiwara I (1994) Optimal rectangular plate and shallow shell topologies using thickness distribution or homogenization. Comput Methods Appl Mech Eng 115: 111–124

Wang MY, Wang XM (2004) Color level sets: a multi-phase level set method for structural topology optimization with multiple materials. Comput Methods Appl Mech Eng 193: 469–496

Wang MY, Wang XM, Guo DM (2003) A level set method for structural topology optimization. Comput Methods Appl Mech Eng 192:227–246

Youn SK, Park SH (1997) A study on the shape extraction process in the structural topolgy optimization using homogenized material. Comput Struct 62:527–538

Yue W, Lin CL, Patel VC (2005) Coherent structures in open-channel flows over a fixed dune. J Fluids Eng 127:858–864